ORIGINAL ARTICLE

Non-oxidative thermal decomposition of oil palm empty fruit bunch pellets: fuel characterisation, thermogravimetric, kinetic, and thermodynamic analyses

Bemgba B. Nyakuma[1] · Syieluing Wong[2] · Olagoke Oladokun[2]

Abstract

The pre-treatment and pelletisation of oil palm empty fruit bunches (OPEFB) can potentially improve its biofuel properties for efficient thermal energy recovery. Therefore, this paper examines the physicochemical, thermal, kinetic, and thermodynamic properties of OPEFB pellets as a potential feedstock for pyrolysis. Physicochemical analysis revealed high proportions of carbon, volatiles, and fixed carbon compared to nitrogen and sulphur. Morphological analysis showed that the pellet microstructure is comprised of a dense network of polymeric fibres, whereas its ash has consistently shaped agglomerated particles with fine-textured surfaces. Thermogravimetric analysis (TGA) revealed the OPEFB pellets experienced significant mass loss ($M_L = 72.8$–80.4%) and residual mass ($R_M = 19.6$–27.2%) during thermal decomposition from 30 to 800 °C. The DTG plots revealed thermal decomposition occurred in three stages: I (30–150 °C), II (150–600 °C), and III (600–800 °C) due to drying, devolatilization, and char degradation, respectively. Kinetic analysis showed the activation energy, E_a, ranged from 76.87 to 195.78 kJ/mol, while frequency factor, A, was from 4.77×10^{01} to 1.22×10^{18} min^{-1} for the Flynn-Wall Ozawa and Kissinger-Akahira Sunose models. The highest kinetic parameters were observed at $\alpha = 0.40$, indicating the rate-determining step for OPEFB pellets decomposition under pyrolysis condition occurs at 40% conversion. Thermodynamic analysis showed that thermal decomposition of OPEFB pellets was characterised by the formation of an activated complex, high reactive multiphase first-order reactions, and short reaction times. In conclusion, the results indicate that OPEFB pellets is a potentially suitable feedstock for pyrolysis owing to its excellent fuel properties and environmentally friendly nature.

Keywords Pyrolysis · Oil palm · Empty fruit bunch · Pellets · Thermogravimetry · Kinetics

1 Introduction

The global demand for crude palm oil (CPO) has exponentially increased the cultivation of oil palm (*Elaeis guineensis* Jacq.) in Malaysia. In 2017, external trade of palm oil and palm oil–based products generated RM74.8 billion of Malaysia's gross national income [1]. Consequently, the palm oil industry is a significant contributor to socio-economic growth and sustainable development in the country [2]. Conversely, the rapid growth of the palm oil industry has created substantial waste disposal and management problems in Malaysia. Typically, the large-scale cultivation and CPO production generate roughly about 83 million tonnes of dry solid oil palm wastes (OPW) annually at various plantations and oil palm mills across the country [3]. The distribution of the solid dry wastes generated in oil palm plantations consists of oil palm fronds, palm leaves, and trunks. However, the oil palm mill-related solid wastes generated include palm mesocarp fibres, palm kernel shell, and oil palm empty fruit bunches (OPEFB) [4]. The most abundant and problematic OPW is OPEFB due to its bulky heterogeneous nature, high moisture content (60%), and alkali metal content [5–7].

✉ Bemgba B. Nyakuma
bbnyax1@gmail.com

1 Hydrogen and Fuel Cell Laboratory, Institute of Future Energy, Universiti Teknologi Malaysia, 81310 Skudai, Johor Bahru, Malaysia

2 School of Chemical and Energy Engineering, Faculty of Engineering, Universiti Teknologi Malaysia, 81310 Skudai, Johor Baru, Malaysia

Similarly, OPEFB is characterised by poor fuel properties such as low calorific value, volumetric, and gravimetric energy density [8].

According to the Agency for Innovation in Malaysia, the volume of wastes generated by the palm oil industry will exceed 100 million dry tonnes by the year 2020 [3]. These outlined projections are based on the rising global demand for CPO, which is currently utilised as feedstock for the production of consumer products as well as biochemicals, biofuels, and biodiesel around the globe [9, 10]. Currently, the solid OPW generated is utilised for organic manure, mulching, soil erosion mitigation, or boiler fuel in various oil palm mills across Malaysia [11–14]. Other studies have examined the potential of OPEFB as polymer composite materials, reinforced fibres, wood or paper products, building materials, among others [15–17]. Despite these milestones, large quantities of OPW remain unutilised and are consequently dumped in open pits or plantation fields, resulting in the ubiquitous stockpiles found in many palm mills around the country. Therefore, there are growing concerns that the lack of decisive action in addressing the growing problems of disposal, management, and accumulation of OPW could result in future socio-economic and environmental challenges [12].

Over the years, numerous policies have been proposed to examine more sustainable strategies to address the growing challenges posed by OPW in Malaysia. One of such policies is the National Biomass Strategy (NBS-2020) promulgated by the government of Malaysia in 2011. The policy aims to address the growing menace of solid wastes disposal and management through the valorisation of the OPWs into high-value bioenergy, biofuels, and biochemical products. Similarly, numerous studies have been reported on the thermochemical conversion of OPW, albeit with limited success. These studies have examined the combustion [18–20], gasification [21, 22], and torrefaction [23, 24] of OPWs. The findings have demonstrated the valorisation of OPWs through these technologies is characterised by low product yields, emission of pollutants, greenhouse gases, and the formation of secondary wastes such as fly or bottom ashes and clinker due to low efficiencies of conversion.

The outlined challenges are ascribed mainly to the poor fuel properties of OPW, particularly OPEFB. The inferior qualities of OPEFB are due to its high heterogeneity, metals, and moisture content along with low heating values, which hamper efficient conversion, transport, and long-term storage [25, 26]. Consequently, OPEFB requires extensive pre-treatment and fuel characterisation to improve its solid biofuel properties for thermochemical conversion through pyrolysis. The process of pyrolysis is one of the most practical approaches for valorising OPWs due to its capacity to thermochemically convert low-value wastes into high value solid, liquid, and gases products. In addition, pyrolysis is an important intermediate process for thermochemical biomass

conversion processes such as gasification and combustion [27]. As such, pyrolysis is a significant predictor of process feasibility, conversion efficiency, emissions profile, products distribution, and wastes residue analysis during biomass valorisation.

Furthermore, pre-treatment through pelletisation is an important step in the utilisation of biomass feedstock for thermochemical energy recovery [28]. Pelletisation is the process of compacting loose biomass species into a solid uniform shape under high pressure and low temperatures [29, 30]. The technique reportedly improves the physicochemical, thermal fuel properties, storage, and transport properties of biomass feedstocks [31, 32]. Therefore, this study seeks to examine the fuel characteristics and pyrolysis of oil palm empty fruit bunches into pellets, hereafter termed, OPEFB pellets for energy recovery and efficient conversion. The fuel characterisation will examine the physicochemical, functional group, microstructure, mineralogical, and thermal fuel properties of OPEFB Pellets. To the best of the authors' knowledge, this is the first comprehensive study that examines the thermodynamic and multicomponent devolatilization kinetic characteristics of any form of oil palm wastes in the literature. It is envisaged that the findings will provide a comprehensive understanding of the fuel properties of OPEFB pellets for future applications in the production of biofuels, biochemicals, and biomaterials through pyrolysis.

2 Materials and methods

2.1 Materials

The OPEFB pellets were acquired from an oil palm processing mill in Kota Tinggi in Johor (Malaysia). The OPEFB pellets were subsequently transported to Universiti Teknologi Malaysia (UTM) for further analysis. Figure 1 presents a

Fig. 1 Oil palm empty fruit bunch (OPEFB) pellets

pictorial depiction of the brown, uniformly shaped, and cylindrical 8-mm diameter OPEFB pellets examined in this study.

Before characterisation, the OPEFB pellets were pulverised in a high-speed crusher (Model: Panasonic Super Dry Mixer Grinder MX-AC400, Malaysia). The pulverised sample was subsequently sifted using a standard laboratory sieve of Mesh size 60 (Brand: W.S. Tyler, Mexico) to obtain homogenous sized particles below 250 μm. Afterwards, the sample was subjected to extensive characterisation to determine its physicochemical, thermal, kinetic, and thermodynamic fuel properties.

2.2 Physicochemical analyses

The elemental composition of the OPEFB pellets was carried out using the CHNS analyser (Model: vario MICRO cube *Elementar Analysensysteme* GmbH, Germany). The analytical procedure was based on the ASTM D5291-10 (2015) standard for determining the elemental CHNS (carbon, hydrogen, nitrogen, and sulphur, respectively) composition of fuels. The proximate fuel properties were determined according to the ASTM standards; D3173-87 (2003) for moisture (M), D3175-07 (2007) for volatile matter (VM) and D3174-04 (2004) for ash (A) in a muffle furnace (Model; Ney Vulcan D-130, USA). The oxygen (O) was then calculated by difference. Lastly, the higher heating value (HHV) was determined based on the ASTM D-2015 standard through an isoperibol oxygen bomb calorimeter (Model: IKA C2000, USA). All tests were repeated three times to ensure the accuracy and reliability of the measurements, which are presented as average values in Table 1.

2.3 Microstructure and mineralogical analyses

The microstructure and mineralogical analyses were performed by scanning electron microscopy (SEM) and energy dispersive x-ray (EDX) spectroscopy, respectively. The SEM-EDX device (Model: JEOL JSM-IT300 LV, Japan) is an expanded pressure scanning electron microscope operated through the Aztec EDX software (Oxford Instruments™, UK). Before each run, the samples were spray deposited on the double-sided epoxy tape pre-placed on 1-cm diameter grain mounts. Next, the SEM samples were mounted on a carbon stub, placed in the sample chamber, and degassed for 15 min to purge moisture and residual gases. The microscope was initiated, and the samples were scanned to obtain the surface micrographs at a magnification of × 1000 using the point ID and mapping technique. On completion, the EDX analysis of the captured zone in the SEM micrograph was performed to determine the quantitative elemental composition. Consequently, the EDX peaks and elemental composition were deduced based on charge balance.

2.4 Metal oxides analysis

The metal oxides composition of the OPEFB pellets ash was determined by X-ray fluorescence (XRF) spectroscopy. Before the XRF analysis, the sample was first pulverised and sieved in a standard 250-μm analytical sieve. The pulverised sample was subsequently oven-dried by heating at 105 °C for 12 h in a muffle furnace (Model: NeyTech Vulcan D-130, USA). Next, the dried sample was converted into ash by heating the sample at 550 °C for 12 h until the brown powdered sample was converted to grey, indicating completion of the ashing process. The XRF analysis was performed using the loose powder method on the Shimadzu Energy Dispersive X-ray Fluorescence (EDXRF) spectrometer (EDXRF Model: EDX-7000, Japan) operated with the PCEDX Navi software. The metal composition was subsequently determined under vacuum based on the settings: 15–50 kV, current 1000 μA, and 0–40 keV. The collimator of size 10 mm with 100 s counting time was used to determine the analytes Al-U, Na-Sc, Rh-Cd, Zn-As, Pb, Cr-Fe, and S-K. On completion, the data on the metal elements were displayed on

Table 1 Physicochemical fuel properties of OPEFB pellets

Fuel characterisation	Element/property	Symbol (units)	Composition of OPEFB pellets
Ultimate analysis	Carbon	C^{db} (wt%)	45.23 ± 0.00
	Hydrogen	H^{db} (wt%)	6.00 ± 0.46
	Nitrogen	N^{db} (wt%)	1.21 ± 0.04
	Sulphur	S^{db} (wt%)	0.13 ± 0.01
	Oxygen	O^{db} (wt%)	47.43 ± 0.41
Proximate analysis	Moisture	M^{ar} (wt%)	7.78 ± 0.18
	Volatile matter	VM^{db} (wt%)	81.53 ± 0.10
	Ash	A^{db} (wt%)	6.28 ± 0.08
	Fixed carbon	FC^{db} (wt%)	12.19 ± 0.18
Calorific analysis	High heating value	HHV^{ar} (MJ/kg)	17.57 ± 0.27

the acquisition software. The results were then retrieved, and the metal oxide composition computed by the PCEDX Navi software [33].

2.5 Functional group analyses

The functional group chemistry of the pulverised OPEFB pellets was examined by Fourier transform infrared (FTIR) spectroscopy. The Shimadzu FTIR analyser (Model: Prestige-21, Japan) used in this study was equipped with an attenuated total reflectance (ATR) attachment. For each run, a small quantity of the pulverised sample (250 μm) was retrieved and placed on the ZnSe prism plate. Each sample was then scanned 20 times at a resolution of 8 cm^{-1} to acquire the spectra in transmittance (T, %) mode from 4000 to 400 cm^{-1} based on Happ-Genzel Apodization. On completion of the 10-s scan, the results were subjected to ATR correction to acquire the FTIR-ATR spectra before analyses in Microsoft Excel© (version 2013).

2.6 Thermal analyses

Thermogravimetric analysis (TGA) of the OPEFB pellets was performed to examine the thermal degradation behaviour, kinetic decomposition parameters, and temperature profile characteristics (TPC) under non-isothermal, non-oxidative (pyrolysis) conditions. The TGA runs were performed on the Netzsch™ TG analyser (Model: TG 209 F3 Tarsus, Germany). For each run, about 9 mg of pulverised OPEFB pellets (250 μm) was placed in an alumina crucible and transferred to the sample holder of the TG analyser. Next, the sample was heated from 30 to 800 °C at the heating rates 5, 10, 15, 20, and 30 °C/min under nitrogen (N$_2$ flow rate 50 ml/min) gas atmosphere. The TGA experiments were performed twice to examine the repeatability of the measurements. However, the replications produced identical results, which did not warrant averaging. Hence, the results presented are based on a single run.

On completion, the raw TG data was recovered and examined using the Netzsch Proteus® software to deduce the mass loss data and temperature profile characteristics (TPC). Consequently, Microsoft Excel (version 2013) was used to plot the mass loss (%) and derivative mass loss (%) data against temperature (°C) to obtain the thermogravimetric (TG, %) and derivative thermogravimetric (DTG, %/min) plots, respectively. The TPC parameters determined from the TG-DTG plots were onset (T_{onset}), peak decomposition (T_{peak}), and offset (T_{end}) temperatures along with mass loss (M_L), and residual mass (R_M).

2.7 Kinetic decomposition analysis

The kinetic parameters activation energy (E_a) and frequency factor (A) for the non-oxidative thermal (pyrolysis)

decomposition of the OPEFB pellets were computed from the Flynn-Wall-Ozawa (FWO) and Kissinger-Akahira-Sunose (KAS) kinetic models. The thermal decomposition of biomass is typically described by the one-step global model in which the material degrades through a single reaction pathway expressed as [34]:

$$Biomass \xrightarrow{k} Volatiles + Char \tag{1}$$

The volatiles consist of the liquid (bio-oil) and gas (condensable and non-condensable components biogases). Based on the model, the degree of conversion (α) for biomass at the temperature (T, K) and time (t, in seconds) is deduced by

$$\alpha = \frac{m_i - m_a}{m_i - m_f} \tag{2}$$

The terms m_i, m_a, and m_f denote the initial mass, instantaneous mass, and final mass of thermally decomposing biomass, respectively. Therefore, the reaction model $f(\alpha)$ for the thermal decomposition of any biomass for a selected order of reaction, n, is given by

$$f(\alpha) = (1-\alpha)^n \tag{3}$$

Furthermore, the temperature dependence of the process is described by the Arrhenius equation:

$$k(T) = A exp\left(\frac{-E_a}{RT}\right) \tag{4}$$

The term $k(T)$ represents the temperature-dependent rate constant; A is the pre-exponential factor (min^{-1}); E_a is the activation energy (kJ/mol); R is the molar gas constant (J/mol K); T is temperature (K). Therefore, the rate of thermal decomposition of OPEFB pellets is given by

$$\frac{d\alpha}{dt} = k(T)f(\alpha) \tag{5}$$

Next, Eqs. 3 and 4 are substituted into Eq. 5 to examine the effect of temperature on the thermal decomposition of the OPEFB pellets, as presented in Eq. 6:

$$\frac{d\alpha}{dt} = A exp\left(\frac{-E_a}{RT}\right)(1-\alpha)^n \tag{6}$$

After separation of variables, the term $\beta = dT/dt$ is introduced to account for thermal decomposition under multiple heating rates. Therefore, Eq. 6 can be written as [35]:

$$\frac{d\alpha}{(1-\alpha)^n} = \frac{A}{\beta} exp\left(\frac{-E_a}{RT}\right)dT \tag{7}$$

By integrating Eq. 7, the fundamental relation for determining the activation energy, E_a, and frequency factor, A, is deduced for thermally decomposing biomass using the

isoconversional models. In this study, the kinetic parameters for the OPEFB pellets decomposition under non-oxidative pyrolysis conditions were examined through the Flynn-Wall-Ozawa (FWO) and Kissinger-Akahira-Sunose (KAS) models. The computations are based on the temperatures (T) corresponding to OPEFB pellets thermal conversion (α) deduced from the mass loss (TG) data.

2.7.1 Flynn-Wall-Ozawa model

The kinetic parameters for the non-oxidative thermal decomposition of OPEFB pellets were deduced from the governing equations of the Flynn-Wall-Ozawa (FWO) model:

$$ln(\beta) = ln\left(\frac{AE_a}{Rg(\alpha)}\right) - 5.331 - 1.052\left(\frac{E_a}{RT}\right) \tag{8}$$

Consequently, plots of $\ln(\beta)$ against 1000/T for $\alpha = 0.10$ to 0.70 were examined to calculate the activation energy, E_a, and frequency factor, A. The E_a and A were computed from the slope ($-1.052 E_a$/R) and intercept $\ln (AE_a/R)$, respectively.

2.7.2 Kissinger-Akahira-Sunose model

Likewise, the activation energy, E_a, and frequency factor, A, for the non-oxidative thermal decomposition of OPEFB pellets were deduced from the governing equations of the Kissinger-Akahira-Sunose (KAS) model:

$$ln\left(\frac{\beta}{T^2}\right) = ln\left(\frac{AR}{g(\alpha)E_a}\right) - \left(\frac{E_a}{RT}\right) \tag{9}$$

Consequently, term $\ln(\beta/T_2)$ was plotted against 1000/T for $\alpha = 0.10$ to 0.70. The E_a and A were computed from the slope -E_a/R and intercept $\ln(AR/E_a)$ of the kinetic plots, respectively.

2.8 Multicomponent analysis

The TG data was subjected to multicomponent devolatilization analyses based on the multicomponent fitting method (MFM) proposed by Hattingh et al. [36] and modified by Oladokun et al. [37]. The method utilises an algorithm to determine the best fit for the pseudocomponents (multicomponent) of thermally decomposing carbonaceous materials under non-oxidative TGA. In this study, the TGA data were computed in MATLAB using the lsqcurvefit function, the Trust-Region-Reflective algorithm, and Levenberg-Marquardt optimisation procedures. The flowchart of the algorithm is presented in Fig. 2 [37].

The multicomponent devolatilization procedure involved importing the TGA data into MATLAB for the simulations. The TGA data for five (5) heating rates (5, 10, 15, 20, and 30 °C/min) was imported into the algorithm to compute the fractional (iso) conversion and devolatilization (dα/dT and

dα/dt) rates. Next, the pseudocomponents (3–10) and initial kinetic parameters (E_a,i, A_i, and ξ_i) were imputed in MATLAB. The lower limit (3) represents the biomass components: hemicellulose, cellulose, and lignin. The symbol E_a,i represents the activation energy, A_i is the frequency factor, and ξ_i is the positive contributing factor. For all simulations, the lower limit was zero (0), and the upper limit was infinity (∞) for the kinetic parameters, whereas ξ was set at unity (1). Once completed, the simulation proceeded to the reaction for-loop and objective function (OBF) minimisation.

Consequently, the kinetic parameters (E_a,i, A_i, and ξ_i) were computed in 200 runs using the lsqcurvefit function and trust-region-reflective algorithm in MATLAB. Next, the resulting kinetic parameters and OBF values were constrained to perform the optimisation. The first of two constraints was executed to determine the positive last contribution factor (ξ) for each run. The second constraint examined the results of the first constraint to minimise the OBF. Hence, the run(s) that satisfied the constraints were considered the optimised kinetic parameters. Based on the optimisation results, the parameters αi, dαi/dT, dαi/dt, and QOF (quality of fit) for each pseudocomponent were calculated. The QOF is a measure of the accuracy of the model that describes the devolatilization and deconvolution of OPEFB pellets during TGA [36]. Hence, the lower the QOF value, the higher the model accuracy. Therefore, the multicomponent devolatilization algorithm (Fig. 2) was utilised to simulate and calculate the QOFs for 3 to 10 pseudocomponents for the non-oxidative multi-heating rate TGA of the OPEFB pellets.

2.9 Thermodynamic analysis

The thermodynamic parameters enthalpy (ΔH), Gibb's free energy (ΔG), and entropy change (ΔS) for the non-oxidative thermal decomposition of the OPEFB pellets were computed from Eqs. 10–12 [38]. The ΔH, ΔG, and ΔS were calculated from the E_a and A of the FWO model and the DTG peak temperature ($T_{peak} = 302.20$ °C or 575.35 K) at 5 °C/min.
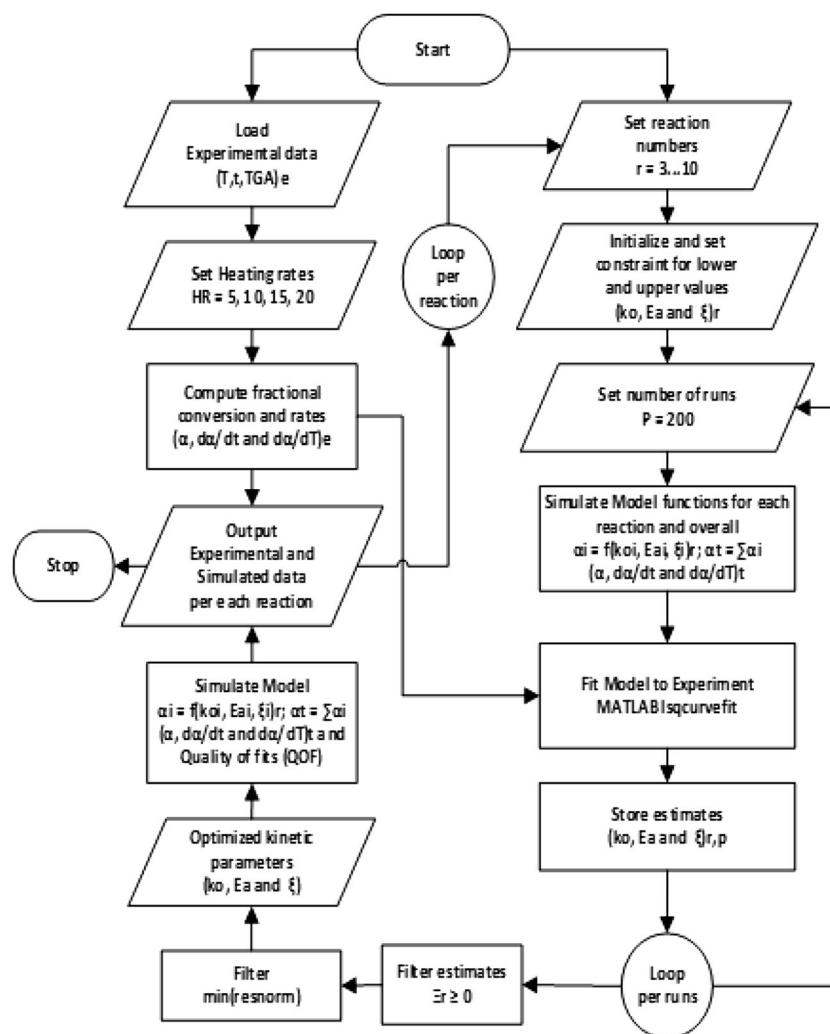
$$\Delta H = E_\alpha - RT \tag{10}$$

$$\Delta G = E_\alpha + RT_{peak} ln\left(\frac{K_B T_{peak}}{hA}\right) \tag{11}$$

$$\Delta S = \frac{\Delta H - \Delta G}{T_{peak}} \tag{12}$$

The terms represent ΔH—enthalpy (kJ/mol), ΔG—Gibb's free energy (kJ/mol), ΔS—entropy change (J/mol), T_{peak}—peak decomposition temperature (°C), K_B—Boltzmann's constant (1.38×10^{-23} J/K), and h—Planck's constant (6.626×10^{-34} Js).

3 Results and discussion

The fuel characterisation of the OPEFB pellets is presented in terms of its physicochemical, microstructure, mineralogical, and thermal properties. The physicochemical properties are presented based on the elemental, proximate, and calorific analyses. However, the microstructural properties present the surface, structural, and mineralogy properties of OPEFB pellets. Lastly, the thermal properties present the degradation behaviour, characteristic temperature profiles, reaction mechanism, kinetic, and multicomponent devolatilization properties of OPEFB pellets.

3.1 Physicochemical properties

Table 1 presents the physicochemical (elemental, proximate, and calorific) fuel properties of OPEFB pellets in dry basis (*d.b*) with the standard deviations for the measurements. The moisture (*M*) content and higher heating value (HHV) are presented in as received (*a.r*) basis.

As observed, the *C*, *H*, and *O* elements are contained in high proportions. According to Yoo et al. [39], the high O content is a characteristic of woody species of biomass. In contrast, the *N* and *S* content are present in low proportions, which could indicate OPEFB pellets have low potential to emit SO_x, NO_x, and NH_x pollutants. In comparison, the values are in good agreement with the properties of empty fruit bunches (EFB), palm kernel shell (PKS), and sawdust (SD) reported in the literature [39, 40]. The reported values are in the range: $C = 41.81–45.93$ wt%; $H = 5.73–6.65$ wt%; $N = 0.68–2.92$ wt%; $S = 0.00–0.16$ wt% and $O = 37.36–46.00$ wt% [39, 40].

Proximate analysis revealed high volatile matter (*VM*) and fixed carbon (*FC*) in addition to low moisture (*M*) and ash (*A*) contents for OPEFB pellets. The high *VM* and *FC* is an indication that the OPEFB pellets have a high content of condensable and non-condensable gases, which could be beneficial to the product yield and distribution during pyrolysis. However, the low *M* and *A* indicate the valorisation of OPEFB pellets could result in efficient conversion, low energy input, and
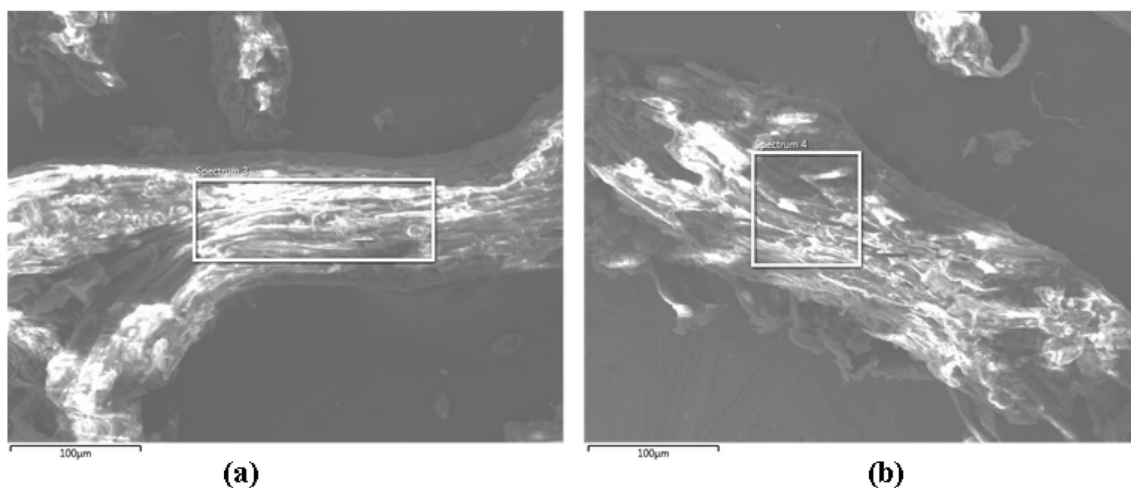
Fig. 3 SEM micrographs for OPEFB pellets

operating costs [41]. In comparison, the proximate properties of the OPEFB pellets are good agreement with empty fruit bunches (EFB), palm kernel shell (PKS), and sawdust (SD) with these ranges: $M = 5.92–9.63$ wt%; $VM = 78.11–86.00$ wt%; $A = 0.58–5.94$ wt%; and $FC = 15.04–19.48$ wt%, as reported in the literature [39, 40, 42]. Lastly, the higher heating value (HHV) of 17.57 MJ/kg is also within the range of 16.95–18.51 MJ/kg reported for similar oil palm biomass in the literature [40].

3.2 Microstructure and mineral properties

Figure 3(a) and (b) present the SEM micrographs for OPEFB pellets, whereas Fig. 4(a) and (b) are the SEM micrographs for OPEFB pellet ash. The SEM analyses were performed to examine the morphological and mineralogical properties of the OPEFB pellets and its ash.

The SEM microstructure of OPEFB pellets in Fig. 3(a) and (b) is characterised by irregular (amorphous) shaped fibrous materials, which are devoid of micro- or mesopores. This

indicates the abundance of a dense network of polymeric lignocellulosic materials such as hemicellulose, lignin, and cellulose components found in most biomass materials. In contrast, the microstructure of ash in Fig. 4(a) and (b) consists of regularly shaped agglomerates with fine-textured and smooth surfaces. According to Romero et al. [43], this indicates the presence of alkali and alkali earth metals (AAEM), which can potentially react with silicon dioxide (SiO_2) to form eutectic mixtures in biomass reactors such as gasifiers and boilers at high temperatures typically above 740 °C. Therefore, the regularly shaped agglomerates may be an indication of or the onset of agglomeration (which causes sintering and fouling) due to the low melting temperature of ash [44].

To examine the presence of AAEMs and other elements, EDX analysis was performed. Table 2 presents the comparative analysis of the EDX elemental composition of OPEFB pellets and ash on a dry basis (*d.b*) along with the standard deviations for the measurements.

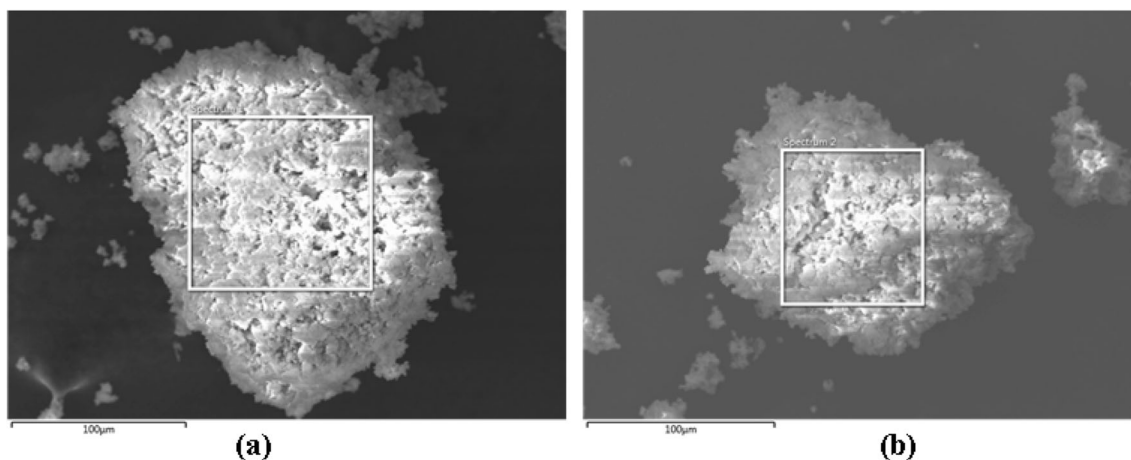The major elements in OPEFB pellets (based EDX peak sizes) are C, O, Al, K, and Si in decreasing order of

Fig. 4 SEM micrographs for OPEFB pellets ash

Table 2 Elemental analysis of OPEFB pellets and ash by EDX

Element	Symbol	OPEFB pellets (wt%)	Ash (wt%)
Aluminium	Al	0.83 ± 1.07	0.81 ± 0.01
Carbon	C	59.29 ± 2.19	17.14 ± 0.67
Calcium	Ca	0.19 ± 0.01	4.49 ± 0.01
Chlorine	Cl	0.10 ± 0.01	2.23 ± 0.00
Copper	Cu	Trace	0.23 ± 0.07
Iron	Fe	Trace	1.08 ± 0.43
Potassium	K	0.80 ± 0.40	25.11 ± 2.47
Magnesium	Mg	0.09 ± 0.02	1.50 ± 0.25
Sodium	Na	Trace	0.15 ± 0.04
Oxygen	O	38.35 ± 2.52	39.78 ± 3.44
Phosphorus	P	0.08 ± 0.03	1.20 ± 0.10
Sulphur	S	0.05 ± 0.07	0.43 ± 0.04
Silicon	Si	0.23 ± 0.22	5.90 ± 0.09

magnitude. This reveals that the OPEFB pellets are predominantly composed of carbonaceous materials due to the high C, O content in addition to oxides of Al, K, and Si. In contrast, the major elements in the ash, as observed in Fig. 4(b) are O, K, C, Si, and Ca in decreasing order of magnitude. The findings indicate the presence of higher concentrations of the oxides of K, Si, and Ca compared to the OPEFB pellets. Lastly, the presence of C in ash indicates the presence of unburned or residual carbon due to incomplete combustion. On the other hand, the elemental composition of the ash consists of Al, C,

Table 3 Metal oxide composition of OPEFB pellets ash

Metal oxides detected	Formulae of detected oxides	OPEFB pellets ash (wt%)
Aluminium oxide	Al_2O_3	3.50 ± 1.24
Calcium oxide	CaO	5.73 ± 0.14
Chlorine	Cl	0.07 ± 0.00
Chromium oxide	Cr_2O_3	0.07 ± 0.00
Copper oxide	CuO	0.02 ± 0.00
Iron oxide	Fe_2O_3	2.05 ± 0.06
Potassium oxide	K_2O	80.13 ± 1.03
Magnesium oxide	MgO	1.03 ± 0.00
Manganese oxide	MnO	0.05 ± 0.00
Niobium oxide	NiO	0.01 ± 0.00
Phosphorus oxide	P_2O_5	1.56 ± 0.04
Rubidium oxide	Rb_2O	0.01 ± 0.00
Silicon oxide	SiO_2	5.51 ± 0.02
Sulphur oxide	SO_3	0.10 ± 0.00
Strontium oxide	SrO	0.01 ± 0.00
Titanium oxide	TiO_2	0.10 ± 0.00
Zinc oxide	ZnO	0.03 ± 0.00
Zirconium oxide	ZrO_2	0.01 ± 0.01

Ca, Cl, Cu, Fe, K, Mg, Na, O, P, S, and Si. However, the OPEFB pellets also contain the typical ash-forming elements except for Cu, Fe, and Na, which were detected trace amounts.

Furthermore, the percentage elemental concentration of all elements except C and Al increased markedly after ashing. This observation may be due to mineralogical enrichment or leaching during the conversion of biomass organic matter to ash. Various studies [45, 46] have confirmed that the high concentration of mineral elements in biomass and its derived ashes is due to soil enrichment along with the decomposition of organic matter, extraneous materials, and cellulose. However, the presence of alkali salts of Na, K, Cl, and AAEMs oxides reportedly causes sintering, fouling, and bed materials agglomeration during biomass conversion [44, 47]. Hence, it is crucial to identify the AAEM oxides and their effects on OPEFB pellets conversion.

3.3 Metal oxide properties

The composition of alkali and alkali earth metal (AAEM) oxides in the OPEFB pellets ash was determined by X-ray fluorescence (XRF) spectroscopy and presented in Table 3 along with the standard deviations for the measurements. The results revealed the presence of Al_2O_3, CaO, Cl, Cr_2O_3, CuO, Fe_2O_3, K_2O, MgO, MnO, NiO, P_2O_5, Rb_2O, SiO_2, SO_3, SrO, TiO_2, ZnO, and ZrO_2 at different concentrations. The major oxides detected during XRF analysis were MgO, P_2O_5, Fe_2O_3, Al_2O_3, SiO_2, CaO, and K_2O in increasing order from 1.03 wt% (MgO) to 80.13 wt% (K_2O). In contrast, the lowest oxide concentrations detected were CuO, Rb_2O, ZrO_2, SrO, and NiO in decreasing order from 0.02 wt% (CuO) to 0.01 wt% (NiO).

In general, the results revealed numerous metal (AAEMs) and non-metal (S, Cl, and Br) oxides were detected in major and trace amounts, respectively. The findings indicate a good agreement between the XRF and EDX analyses. The presence of AAEMs can influence the suitability of biomass feedstock for energy recovery. Furthermore, numerous studies have demonstrated that oil palm wastes with high AAEM content can cause fouling, sintering, and agglomeration during utilisation [21, 48].

3.4 Functional group properties

The chemical and structural compositions of OPEFB pellets were analysed by Fourier transform infrared - attenuated total reflectance (FTIR-ATR) spectroscopy. Figure 5 presents the FTIR-ATR spectrum of OPEFB pellets scanned from 4000 to 400 cm^{-1}. As observed, the FTIR spectrum displays several bands and peaks of various intensities, which represent the functional groups in the OPEFB pellets based on the high-energy and fingerprint regions.
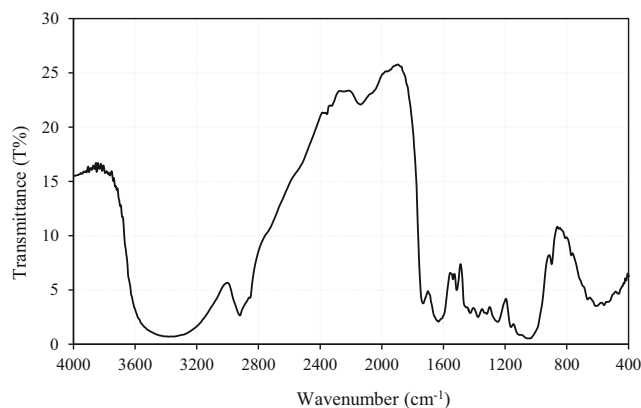
Fig. 5 FTIR spectrum of OPEFB pellets

Fig. 7 DTG plots for OPEFB pellets pyrolysis

The high-energy region is typically characterised by bands or peaks ranging from 4000 to 1500 cm^{-1} of the spectrum. A broad band from 3650 to 3000 cm^{-1} is attributed to the free or intermolecular bonded –OH groups of alcohols, phenols, lignin, and other carbohydrates [49]. However, the band can also be ascribed to the symmetric and asymmetric stretching vibrations associated with surface-bound water [50]. The sharp peaks observed at 2920 cm^{-1}, 2858 cm^{-1}, and 1423 cm^{-1} are due to the symmetric and asymmetric C-H stretching vibrations of aliphatic –CH$_3$– and –CH$_2$– groups [51], which indicate the presence of lignin and extractives. Furthermore, the medium intensity bands observed at 2353 cm^{-1}, 2326 cm^{-1}, and 2137 cm^{-1} are due to the −C≡N–, or –C≡C– stretching vibrations of nitriles or alkynes, which occur in heterocyclic compounds. The typical C=O stretching vibration of carboxylic acids, ketones, esters, and aldehydes were observed at 1728 cm^{-1} and 1377 cm^{-1} [52]. Lastly, the medium-broad peak observed at 1631 cm^{-1} is due to the –C=C– stretching vibrations of alkenes or similar unsaturated compounds.

The fingerprint region, on the other hand, is characterised by IR absorptions in the region 1500–400 cm^{-1}. The sharp peak at 1512 cm^{-1} is attributed to the in-ring –C-C– stretching
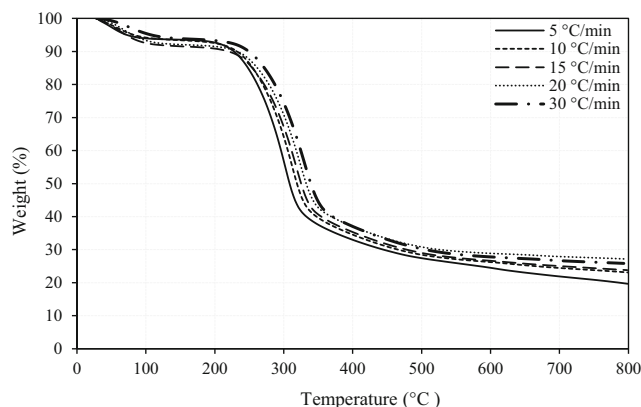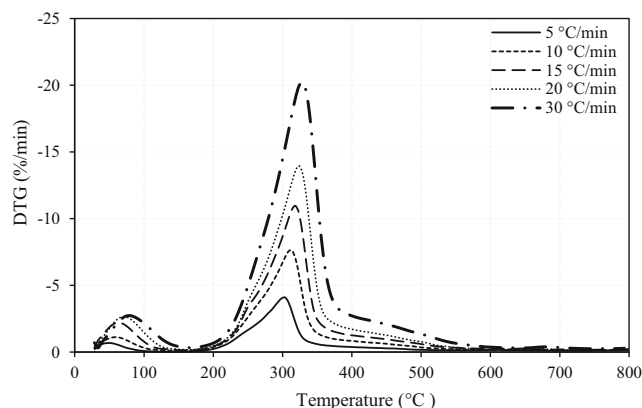
vibrations of unsaturated aromatic groups [53]. The characteristic –C≡N– stretching vibrations of aliphatic amine groups was observed at 1249 cm^{-1}. The broad band at 1037 cm^{-1} can be assigned to the C-O-H, C-O-R, or O-CH$_3$ vibrations observed in the guaiacyl monomers and pyranose rings of cellulose and hemicellulose [54]. Furthermore, the sharp peak observed at 898 cm^{-1} can be attributed to the –C-H– groups in aromatic compounds. The weak absorption bands observed from 900 to 600 cm^{-1} are due to monocyclic, polycyclic, or substituted aromatic groups. Overall, the FTIR analysis revealed that the chemical structure of OPEFB pellets is due to the functional group contributions from alcohols, aldehydes, aliphatic, aromatics, esters, and ketone compounds in its structure.

3.5 Thermal properties

The thermal properties of OPEFB pellets were examined at 5, 10, 15, 20, and 30 °C/min from 30 to 800 °C under nitrogen (N$_2$) conditions through TGA, as presented in the TG and DTG plots in Figs. 6 and 7, respectively.

As observed, TG analysis resulted in a progressive loss of mass as depicted by the downward sloping "Z" shaped curves at various heating rates. This observation indicates that the increase in temperature resulted in step-wise thermal degradation of the lignocellulosic components of the samples. Furthermore, there was a shift in the TG plots to the right with increasing heating rate from 5 to 30 °C/min, which is typically ascribed to the thermal-time lag that occurs during the thermal decomposition of biomass at different heating rates [55]. As a result, the time required by the sample to attain equilibrium temperature during TGA is shortened, resulting in higher temperature profile characteristics (TPC). To examine this effect, the TPCs onset temperature (T_{onset}), offset temperature (T_{end}), mass loss (M_L), and residual mass (R_M) for the pyrolytic decomposition of OPEFB pellets were inferred from the TG plots, as presented in Table 4.

Fig. 6 TG plots for OPEFB pellets pyrolysis

Table 4 Pyrolysis temperature characteristics of OPEFB pellets

Heating rate (°C/min)	Onset T_{Onset} (°C)	Offset T_{End} (°C)	Mass loss (M_L, %)	Residual mass (R_M, %)
5	252.70	332.60	80.36	19.64
10	260.80	346.30	76.91	23.09
15	267.30	353.00	76.19	23.81
20	272.30	360.30	72.82	27.18
30	276.40	368.00	74.18	25.82

As observed, the T_{onset} increased from 252.70 to 276.40 °C, whereas the T_{end} occurred between 332.60 and 368.00 °C with increase in the heating rates. However, the mass loss (M_L) exhibited a decreasing trend from 80.36 to 72.82% as the decomposition time decreased from 154 to 26 min. The decrease in M_L rate accounts for the high residual mass (R_M), which increased from 19.64 to 27.18% at higher heating rates during TGA. Overall, the results demonstrate that the increase in heating rates considerably influenced the thermal degradation, decomposition behaviour, and TPCs of the OPEFB pellets as similarly reported in the literature [56]. The detailed description of the reaction pathway for the pyrolytic decomposition of the OPEFB pellets was deduced through the DTG plots, as presented in Fig. 7.

As observed, the DTG plots consist of two sets of peaks: a set of small symmetric peaks from 30 to 150 °C and another set of large asymmetric peaks in the region from 150 to 600 °C. These findings indicate that the thermal decomposition processes occurred in three (3) stages, namely stage I—(30–150 °C), stage II—(150–600 °C), and stage III—(600–800 °C). The first stage was characterised by mass loss from 30 to 150 °C, due to drying or removal of water molecules (bound by surface tension) and light volatiles [55, 56]. The average mass loss during this stage was 7.78%, which reveals an excellent agreement with the moisture content ($M = 7.78$%) of the OPEFB pellets determined by proximate analysis (see Table 1).

The second stage was characterised by significant mass loss between 150 and 600 °C as typified by the larger sized DTG peaks. However, the study by Yiin et al. [56] observed the second stage for OPEFB degradation to be between 150 and 450 °C, which could be ascribed to the chemical pre-treatment and lower TGA temperature range adopted in their study. In this present study, the average mass loss during this stage was 65.38%, which is somewhat below the volatile matter ($VM = 81.53$%) reported in Table 1. Typically, the mass loss in this region is ascribed to thermal decomposition of hemicellulose (160–360 °C), cellulose (240–390 °C), and other volatile compounds in the biomass structure [57]. Hence, this stage can be termed the active region of pyrolysis or devolatilization. The results also demonstrate that higher temperatures or slower heating rates are required for complete thermal decomposition of the volatile compounds in the OPEFB pellets.

Lastly, the mass loss from 600 to 800 °C was characterised by prolonged "tailing" but no peaks, as seen after the devolatilization region. This stage of the process pyrolysis can be partly ascribed to char degradation reactions, which occur over a wide temperature range from 80 to 900 °C and attributed to lignin decomposition. Yiin et al. [56] reported OPEFB degradation occurred from 450 to 600 °C in this stage, which was not characterised by distinct primary structure for the degradation of lignin. The effects of temperature and higher heating rates on the mass loss rates (MLR) and peak decomposition temperatures for drying ($T_{peak-dry}$) and devolatilization ($T_{peak-dev}$) were also examined, as presented in Table 5.

The peak decomposition temperatures ($T_{peak,dry}$) and the mass loss rate (MLR) in the drying region ranged from 49.00 to 78.30 °C and 0.68%/min to 2.73%/min, respectively.

Table 5 Pyrolysis DTG peak temperatures for OPEFB pellets

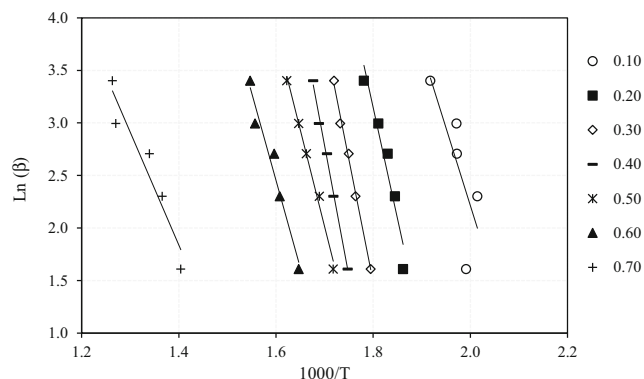| Stage	Drying (30–150 °C)		Devolatilization (150–600 °C)	
Heating rate (°C/min)	$T_{peak,dry}$ (°C)	MLR at $T_{peak,dry}$ (%/min)	$T_{peak,dev}$ (°C)	MLR at $T_{peak,dev}$ (%/min)
5	49.00	0.68	302.20	4.11
10	59.00	1.12	311.60	7.65
15	63.10	2.21	318.00	10.96
20	70.50	2.65	323.40	13.94
30	78.30	2.73	327.80	20.23

Fig. 8 FWO kinetic plots for OPEFB pellets pyrolysis

However, the peak decomposition temperatures ($T_{peak,dev}$) and mass loss rate (MLR) in the devolatilization region ranged from 302.20 to 327.80 °C and 4.11 to 20.23%/min, respectively. This demonstrates that devolatilization resulted in a higher mass loss and extensive-time compared to drying. Therefore, this stage (devolatilization) can be termed the rate-determining step of the process. To validate this, a detailed assessment of the kinetic decomposition of OPEFB pellets was carried out using the isoconversional kinetic analyses.

3.6 Kinetic decomposition properties

The thermal decomposition kinetics of OPEFB pellets was examined using TGA data. Therefore, the activation energy (E_a) and frequency factor (A) for the pyrolysis of OPEFB pellets were deduced from the plots of the Flynn-Wall-Ozawa (FWO) and Kissinger-Akahira-Sunose (KAS) models for conversions $\alpha = 0.10$ to 0.70, as presented in Figs. 8 and 9, respectively.

The kinetic plots for FWO and KAS revealed sets of identical parallel lines, which according to Abrishami et al. [58] indicates the pellet decomposition is characterised by rapidly occurring first-order reactions. Furthermore, the findings indicate that the process is occurring in three stages: $\alpha = 0.0$–0.10, 0.20–0.60, and above 0.70, which represent drying, devolatilization, and char decomposition, respectively, as
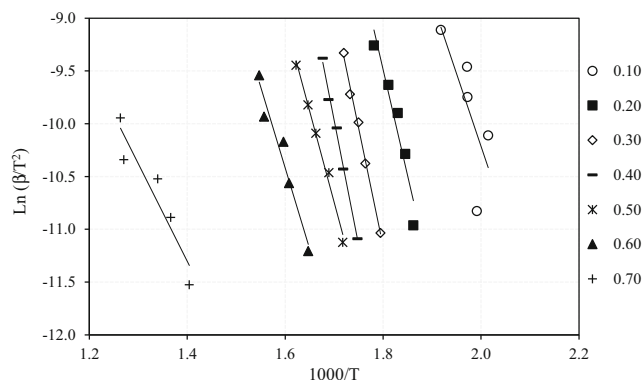

Fig. 9 KAS kinetic plots for OPEFB pellets pyrolysis

earlier reported during TG-DTG analyses. This is based on the ordered arrangement of the identical set of parallel lines observed at α from 0.20 to 0.60 and the isolated values $\alpha = 0.10$ and $\alpha = 0.70$. The findings of this study are thus in good agreement with the global model for kinetic reactions, which states that biomass undergoes pyrolysis into solid, liquid, and gas products based on rapidly occurring first-order reactions. Based on this theory, the E_a and A for OPEFB pellets were computed from the slope and intercept of the plots in Figs. 8 and 9, as presented in Table 6.

For the FWO model, the E_a ranged from 84.97 to 195.33 kJ/mol or 146.63 kJ/mol on average, whereas A was from 2.12×10^{06} to 1.22×10^{18} min^{-1} or 2.42×10^{17} min^{-1} on average. For the KAS model, the E_a was from 76.87 to 195.78 kJ/mol or an average of 144.30 kJ/mol whereas A was ranged between 4.77×10^{01} and 2.68×10^{14} min^{-1} or an average value 5.22×10^{13} min^{-1}. In comparison, the kinetic values of OPEFB pellets in this study were compared with our previous study [59]. In the present study, the thermal and kinetic analyses of OPEFB pellets was performed from 30 to 800 °C based on five heating rates (5, 10, 15, 20, 30 °C/min) whereas it was from 30 to 1000 °C based on only three heating rates (5, 10, 20 °C/min). The findings revealed that the present study has a lower average activation energy ($E_a = 146.63$ kJ/mol) and frequency factor (2.42×10^{17} min^{-1}) values compared to 160.21 kJ/mol and 1.38×10^{24} min^{-1}. Further comparisons showed that the E_a of the OPEPB pellets at 146.63 kJ/mol (present study) and 160.21 kJ/mol [59] are lower the reported values for cornstalk (206.40 kJ/mol), oak tree (236.20 kJ/mol), and sawdust (232.60 kJ/mol) in the literature [60]. However, the results of this study are somewhat higher than the values of 80–94.80 kJ/mol reported for the chemical pre-treatment of OPEFB using sucrose, choline chloride, and monosodium glutamate based low-transition-temperature mixtures (LTTMs) in the literature [56]. The results confirm that biomass pre-treatments either in chemical or physical such as pelletisation can significantly influence its thermochemical fuel properties.

Furthermore, the thermal analysis at higher temperatures and lower heating rates in the previous study [59] yielded a lower mass of residuals from 11.03 to 22.02% compared to 19.64–27.18% in the present study at the comparative heating rates of 5, 10, and 20 °C/min. Since the mass of residuals is an indicator of the potential biochar product from biomass pyrolysis, it can be reasonably surmised that lower temperature (800 °C) and higher heating rates favour the thermal degradation of the OPEFB pellets under the non-oxidative conditions examined in this study. Furthermore, the results of this study indicate that the kinetic parameters fluctuated significantly as the temperature and heating rates were varied during the non-oxidative decomposition of the OPEFB pellets. For both models, there was a rapid rise in the kinetic parameters at different conversion rates from $\alpha = 0.10$ to 0.60 before

Table 6 Kinetic parameters for OPEFB pellets pyrolysis

Conversion α	FWO model			KAS model		
	R^2	E_a (kJ/mol)	A (min^{-1})	R^2	E_a (kJ/mol)	A (min^{-1})
0.10	0.5936	116.76	4.43×10^{12}	0.5587	114.36	4.46×10^{08}
0.20	0.9295	167.28	4.08×10^{16}	0.9220	166.85	7.39×10^{12}
0.30	0.9944	185.42	4.33×10^{17}	0.9939	185.60	9.02×10^{13}
0.40	0.9944	195.33	1.22×10^{18}	0.9939	195.78	2.68×10^{14}
0.50	0.9913	145.42	1.64×10^{13}	0.9900	143.03	1.87×10^{09}
0.60	0.9597	131.20	2.54×10^{11}	0.9531	127.59	2.11×10^{07}
0.70	0.9157	84.97	2.12×10^{06}	0.8884	76.87	4.77×10^{01}
Average	0.9112	146.63	2.42×10^{17}	0.9000	144.30	5.22×10^{13}

dropping at $\alpha = 0.70$. This may be attributed to the complex composition of the pellets and the multi-step kinetic reactions that occur during TGA [38].

The lowest E_a values of 84.97 kJ/mol and 76.87 kJ/mol were observed for FWO and KAS, respectively, which indicates a high rate of pyrolytic decomposition of OPEFB pellets at $\alpha = 0.70$ (70% conversion). However, the highest E_a values, 195.33 kJ/mol and 195.78 kJ/mol observed for FWO and KAS, respectively, occurred at $\alpha = 0.40$. This demonstrates that the pyrolytic decomposition is slow at 40% conversion. Therefore, the conversion of the OPEFB Pellets at $\alpha = 0.40$ can be defined as the rate-limiting step of the process. As stated earlier, the conversion of biomass during this stage is dominated by the devolatilization of hemicellulose, cellulose, and lignin. As such, the process requires high energy input (E_a) due to the slow process of bond breaking and evolution of volatile compounds, which accounts for the high-frequency factors (A) observed at $\alpha = 0.40$ reported in Table 6.

Next, the correlation between the parameters E_a and A for FWO and KAS was examined to detect the effect of kinetic compensation during kinetic analyses. The results for FWO

and KAS models are presented in Figs. 10 and 11, respectively.

As observed, the activation energy, E_a, increased with increasing frequency factor, A, for both the FWO and KAS models with the highest values observed at $\alpha = 0.40$ (40% conversion). According to the kinetic compensation effect (KCE) theory, an increase or decrease in the E_a of thermally decomposing biomass is compensated by a simultaneous increase or decrease in A [61]. This demonstrates that the effect of KCE was evident during the thermal decomposition of the OPEFB pellets in this study. In principle, reactions with high E_a values are typically slow. Hence, the system adjusts to counteract this effect by increasing the effective collisions, which result in a higher frequency factor (A) [62]. The numerical representation of the KCE is [62]:

$$Log\ A = aE_a + b \tag{13}$$

The terms A, E_a, a, and b represent the frequency factor (min^{-1}), activation energy (kJ/mol), whereas a and b are the
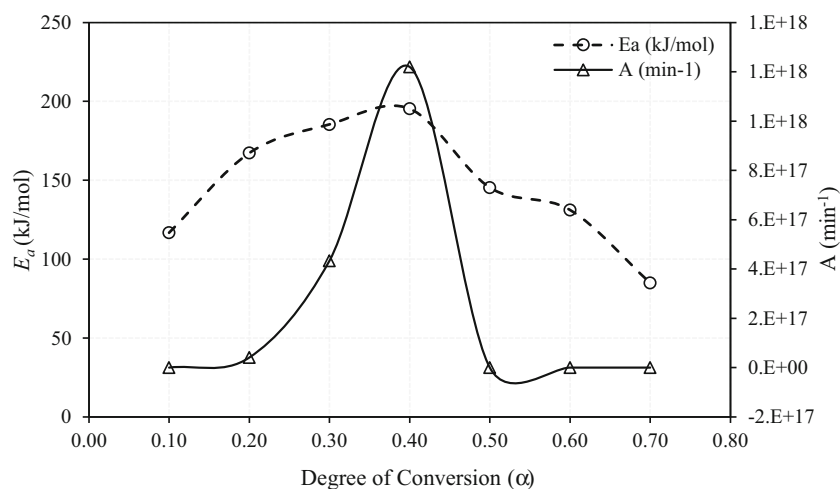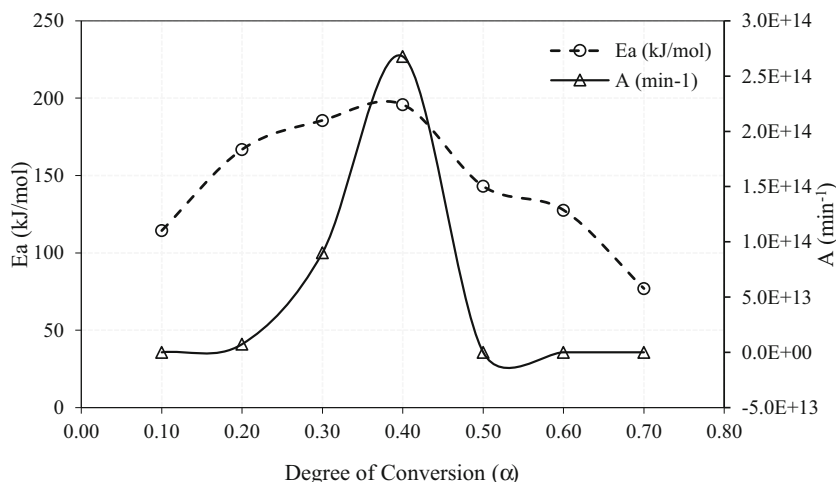

Fig. 10 KCE plots for the FWO kinetic model

Fig. 11 KCE plots for the KAS kinetic model

compensation constants. Based on Eq. 13, the plots of Log A against E_a are presented in Fig. 12.

As observed in Fig. 12, there is a linear relationship between the natural logarithm of frequency factor (A) and the activation energy (E_a) for the pyrolytic decomposition of OPEFB pellets. Based on the plots, the compensation constants for FWO were $a = 0.1027$ and $b = -1.3547$ with an R^2 of 0.9349, whereas for KAS $a = 0.1042$ and $b = -5.2942$ with an R^2 of 0.9439.

3.7 Multicomponent properties

The multicomponent devolatilization analysis was performed on the TG-DTG plots for OPEFB pellets based on the algorithm in Fig. 2. The simulation was performed to determine the number of pseudocomponents, $n = 3$–10 under five heating rates ($\beta = 5$ °C/min to 30 °C/min). Based on this, the quality of fit (QOF, %) was determined as presented in Table 7.

As stated earlier, the QOF is a measure of the accuracy of the model calculated from the optimisation algorithm in Fig. 2 [37]. Based on the results, the QOF for 5 °C/min was from

2.27 to 5.98. For 10 °C/min, the QOF value was from 1.31 to 3.24 and from 1.40 to 2.55 for 15 °C/min. Also, the QOF values were from 1.03 to 2.06 for 20 °C/min and from 1.02 to 2.47 for 30 °C/min. Lastly, the average values for the QOFs for 5, 10, 15, 20, and 30 °C/min were 3.51, 2.01, 1.90, 1.31, and 1.41, respectively. In principle, the lower the QOF values deduced, the higher the accuracy of the simulation. Therefore, the heating rate with the lowest QOF is considered the most reliable for further analysis. To determine the lowest values for QOF, a profile of the QOF for each pseudocomponent was plotted for the heating rates (5–30 °C/min), as presented in Fig. 13.

As observed, the QOF decreased as the number of pseudocomponents and heating rates increased from 5 to 30 °C/min. The highest overall QOF was 3.26 for 3 components, whereas the lowest QOF was 1.45 for 10 components with increasing heating rates. This indicates that the best fit was observed at 10 components. Based on heating rates, the lowest QOF values 2.27%, 1.31%, and 1.02% were observed at 5 °C/min, 10 °C/min, and 30 °C/min for 10 pseudocomponents, respectively. However, the lowest values for 15 °C/min and 20 °C/min were observed for 7 pseudocomponents, corresponding to 1.40% and 1.03%.
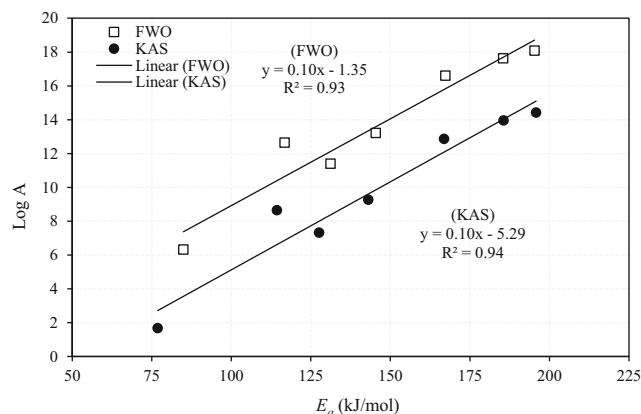

Fig. 12 KCE plots of log A against E_a

Table 7 Quality of fit (QOF) for the pseudocomponents

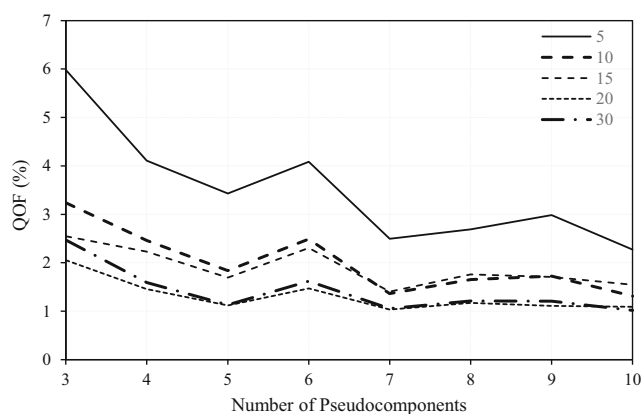| Heating rates (°C/min)	Quality of fit (QOF, %) for the pseudocomponents							
	3	4	5	6	7	8	9	10
5	5.98	4.11	3.43	4.08	2.50	2.69	2.99	2.27
10	3.24	2.46	1.84	2.49	1.36	1.65	1.72	1.31
15	2.55	2.23	1.69	2.31	1.40	1.76	1.71	1.54
20	2.06	1.45	1.12	1.47	1.03	1.17	1.11	1.09
30	2.47	1.59	1.13	1.62	1.06	1.21	1.21	1.02
Total QOF	3.26	2.37	1.84	2.39	1.47	1.70	1.75	1.45

Fig. 13 QOF profiles for the selected pseudocomponents

Figures 14, 15, 16, 17, and 18 present the pseudocomponent plots for OPEFB pellets for different heating rates at best QOF. As observed, the plots show a good correlation between the model and experimental data. Likewise, the results revealed that the deconvolution and devolatilization of the DTG peaks resulted in numerous pseudocomponents. The pseudocomponents represent the lignocellulosic components of biomass which typically decompose into solid, liquid, and gaseous products during pyrolysis.

As earlier described, the pyrolytic thermal decomposition of the OPEFB pellets occurs in three (3) stages I—drying (30–150 °C), II—devolatilization (150–600 °C), and III—char decomposition (600–800 °C). Using Fig. 18, the profile with the best QOF, it can be surmised that components n10 occurred in stage I, the pseudocomponents n1, n3–n9 in stage II, and lastly, n2 occurred in stage III. Therefore, the pseudocomponent peak n10 can be ascribed to water molecules. However, the peaks n5 and n6 can be ascribed to hemicellulose, which usually decomposes from 160 to 360 °C. Furthermore, this is corroborated by the presence of the hemicellulose shoulder peak typically observed for biomass fuels between 300 and 310 °C [63, 64] or
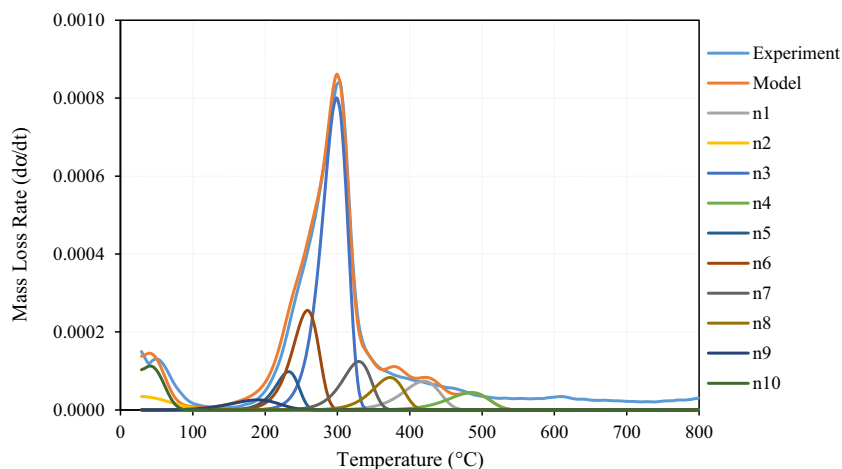
305 °C for OPEFB pellets as observed in this study. Besides, the peaks n3 and n7 observed in the temperature range from 240 to 390 °C can be attributed to the cellulose. Lastly, the other pseudocomponents n1 and n3-n9 in stage II can be ascribed to the presence of extractives or other spurious components [36] resulting from the OPEFB pellets decomposition in the study.

Based on the results of the multicomponent devolatilization and deconvolution, the kinetic parameters; activation energy (E_a), frequency factor (A), and positive contribution factor (ξ) of the pseudocomponents were deduced. The kinetic parameters were deduced for the model with the lowest fit (QOF = 1.02%), which corresponds to 10 components at 30 °C/min. The summary of the results is presented in Table 8.

The activation energy (E_a) ranged from 1.50 to 16.68 kJ/mol^{-1}, whereas the frequency factor was from 6.96×10^{-09} to 1.18×10^{04} min^{-1} and contribution factor (ξ) was from 0.03 to 0.43. The overall sum of the kinetic parameters was $E_a = 115.71$ kJ/mol^{-1}, $A = 1.57 \times 10^{04}$ min^{-1}, and $\xi = 1$. As observed, the kinetic values for the pseudocomponents are lower than the averaged isoconversional values 145.46 kJ/mol^{-1} for E_a and 1.21×10^{17} min^{-1} for A for OPEFB pellets decomposition. The observed 29.75 kJ/mol difference for E_a and 1.21×10^{17} min^{-1} for A can be attributed to the non-inclusion of the conversions in the range $0.70 < \alpha < 0.10$, which accounts for the higher values.

3.8 Thermodynamic properties

The thermodynamic parameters enthalpy (ΔH), Gibb's free energy (ΔG), and entropy change (ΔS) for the OPEFB pellets decomposition were examined. The values were calculated from the kinetic parameters E_a and A of the Flynn-Wall-Ozawa (FWO) model and peak decomposition temperature $T_{peak} = 303.20$ °C (575.35 K) at the heating rate of 5 °C/min. The calculated values for ΔH, ΔG, and ΔS for the OPEFB pellets pyrolysis are presented in Table 9.

Fig. 14 Deconvolution for 10 pseudocomponents at 5 °C/min

Fig. 15 Deconvolution for 10 pseudocomponents at 10 °C/min
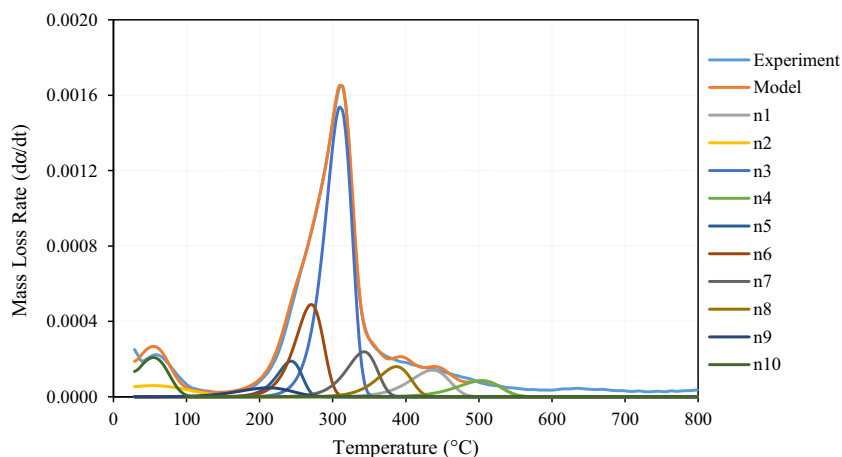
As observed, the enthalpy (ΔH) ranged from 79.05 to 190.57 kJ/mol; Gibb's free energy (ΔG) was from 298.71 to 538.59 kJ/mol, and lastly, the entropy change (ΔS) was between -348.02 and -219.65 J/mol. Hence, the average thermodynamic values are enthalpy ($\Delta H = 141.79$ kJ/mol), Gibb's free energy ($\Delta G = 441.62$ kJ/mol), and entropy change ($\Delta S = -299.83$ J/mol). Based on the results, the condition Gibb's free energy (ΔG) > enthalpy (ΔH) > entropy change (ΔS) was satisfied as defined by the laws of thermodynamics. In comparison, the average ΔS value (-299.83 J/mol) observed was lower than (-249.52 J/mol) determined for red pepper waste [38]. The negative ΔS values demonstrate that the degree of disorderliness of the initial reactants is higher than the products formed by bond dissociation.

In general, the findings indicate that the decomposition of the fuel occurred through an intermediate step or activated complex near its thermodynamic equilibrium [38]. Consequently, the process is highly reactive, thereby ensuring short reaction times. However, Gibb's free energy (ΔG) and enthalpy (ΔH) change showed that the total energy increase of the system at the approach of the reagents and the formation of the activated complex. Lastly, the results indicate the pyrolytic decomposition of OPEFB pellets is characterised by a high degree of complex, random, and multiphase first-order reactions [38], as earlier surmised based on the findings of Miura, Maki [65].

3.9 Potential applications

The effective utilisation of any potential biomass feedstock is dependent in its physicochemical, mineralogical, thermal, kinetic, and thermodynamic fuel properties. Therefore, the solid fuel properties of OPEFB pellets were examined in this study to ascertain its chemical fuel characteristics, thermal degradation behaviour, and energy recovery potential during conversion. The solid fuel characteristics of OPEFB pellets presented in this study have numerous potential applications.

Firstly, the physicochemical properties of the OPEFB pellets are critical to examining its suitability and selection as feedstock for thermochemical conversion processes.

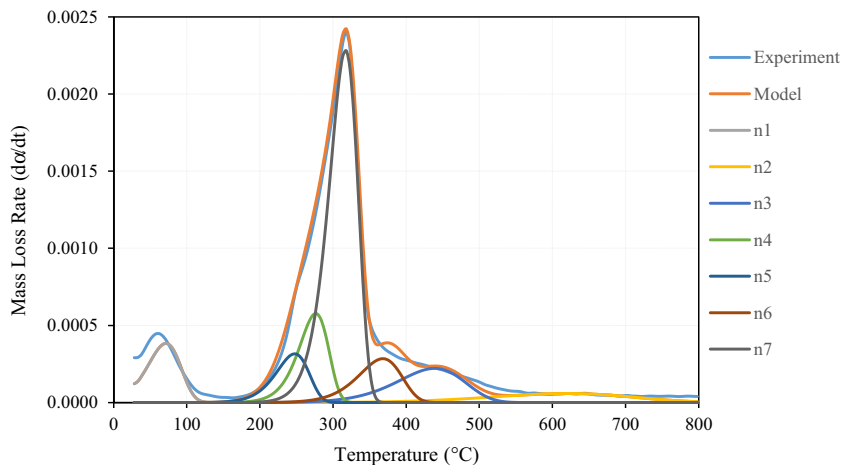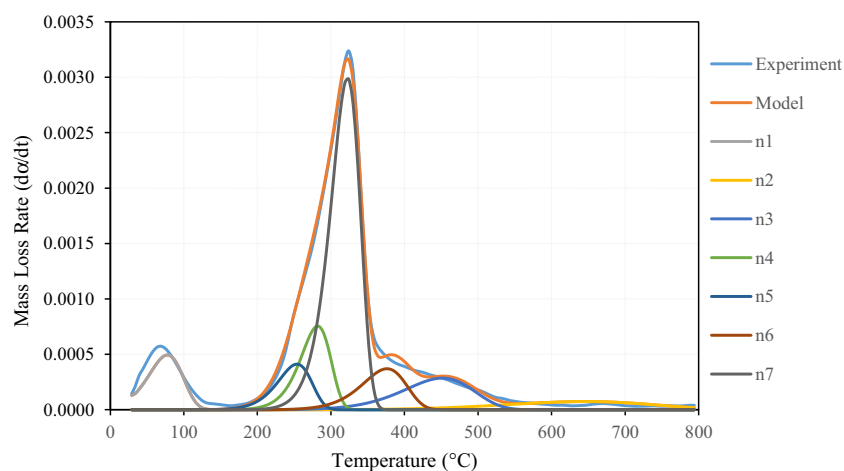**Fig. 16** Deconvolution for 7 pseudocomponents at 15 °C/min

Fig. 17 Deconvolution for 7 pseudocomponents at 20 °C/min

Typically, a good feedstock contains high carbon (> 40 wt%), HHV (> 14 MJ/kg, volatile matter (> 75 wt%) but low oxygen (< 50 wt%), nitrogen (< 12 wt%), sulphur (< 2.3 wt%), and AAEMs [42]. In comparison, the OPEFB pellets examined in this study meet the outlined requirements and hence pose minimal risks to human health, safety, and environment in terms of pollutant emissions from thermal conversion. Despite this, studies have revealed that the storage of pellets results in the off-gassing phenomenon, which releases carbon monoxide (CO) and volatile organic compounds (VOCs) such as hexanal, methanol, and acetone [66]. The long term exposure to CO and VOCs could severely endanger people who work in surroundings where pellets are stored particularly if poorly ventilated.

Furthermore, the comparisons with the DIN 51731 pellet specifications showed that the OPEFB pellets meet the requirements for moisture (< 12 wt%), heating value (17.5–19.5 MJ/kg) along with the length (< 50 mm) and diameter (8 mm) [67, 68]. However, the ash, nitrogen, and sulphur contents fall short of the DIN 51731 pellet specifications for nitrogen (< 0.3 wt%), sulphur (< 0.08 wt%),

ash (< 1.5 wt%), and low AAEMs [67, 68]. The low ash and AAEMs requirement are crucial to the secondary wastes, reactor materials selection, and engineering economics of selected thermochemical processes. This is ascribed to the potential effects of these parameters on operating conditions and technical challenges such as corrosion, agglomeration, and sintering. Overall, the physicochemical fuel characteristics of the OPEFB pellets in this study are within acceptable limits required for biomass feedstock for thermochemical conversion processes such as pyrolysis.

Secondly, the thermal degradation, kinetic decomposition, and thermodynamic fuel characteristics of OPEFB pellets can be applied in the design, optimisation, and scale-up of future thermochemical energy recovery systems. In this study, the thermal, kinetic, pseudocomponent devolatilization, and thermodynamic analyses of the OPEFB pellets was performed to critically examine its solid biofuel properties and provide an empirical basis for comparison with our previous study in the literature [59]. In the present study, the thermal and kinetic analyses

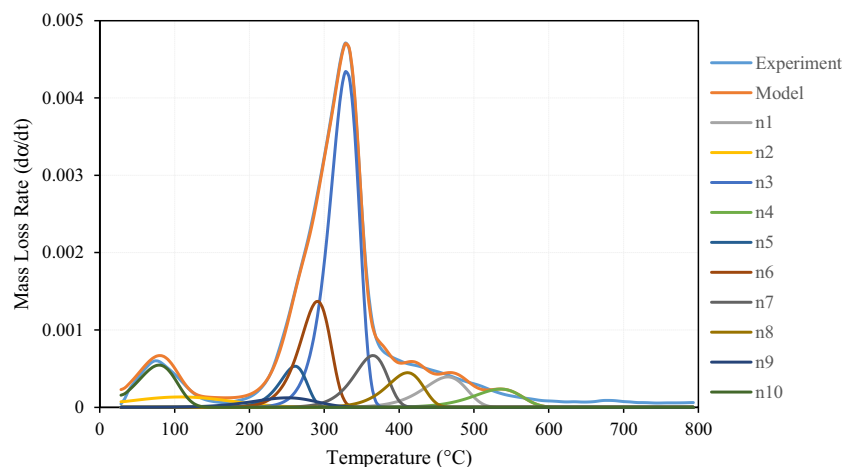**Fig. 18** Deconvolution for 10 pseudocomponents at 30 °C/min

Table 8 Kinetic values for 10 pseudocomponents at 30 °C/min

Pseudocomponent (n)	E_a (kJ/mol)	A (min^{-1})	Contribution factor (ξ)	Stage of pyrolysis
1	15.55	1.72×10^{01}	0.06	II
2	1.50	6.96×10^{-09}	0.04	III
3	15.76	1.18×10^{04}	0.43	II
4	16.68	9.01×10^{00}	0.04	II
5	13.27	2.64×10^{03}	0.05	II
6	12.93	2.27×10^{02}	0.14	II
7	15.18	5.98×10^{02}	0.08	II
8	16.00	3.34×10^{02}	0.06	II
9	5.10	1.34×10^{-05}	0.03	II
10	3.74	6.32×10^{-05}	0.07	I
Sum total	115.71	1.57×10^{04}	1.00	**

of OPEFB pellets were performed at a lower final temperature of 800 °C based on five heating rates (5, 10, 15, 20, 30 °C/min) compared to 1000 °C and three heating rates (5, 10, 20 °C/min) in our previous study [59]. The activation energy (E_a = 146.63 kJ/mol) and frequency factor (2.42×10^{17} min^{-1}) values in this study are clearly lower on average compared to 160.21 kJ/mol and 1.38×10^{24} min^{-1}. Therefore, it can be realistically inferred that the OPEFB pellets thermal degradation under the non-oxidative conditions is favoured by lower temperatures and higher heating rates. However, the thermodynamic parameters indicate the OPEFB pellets undergo rapid thermal degradation which requires short reaction times. Ultimately, these findings indicate the OPEFB pellets are highly reactive which eliminates the need for specialised equipment, operating conditions or additives such as catalysts which typically increase the operational costs of utilising biomass as feedstock for thermal conversion processes.

Table 9 Thermodynamic properties of OPEFB pellets decomposition

Conversion (α)	ΔH (kJ/mol)	ΔG (kJ/mol)	ΔS (J/mol)
0.10	112.58	400.10	−287.52
0.20	162.81	494.29	−331.48
0.30	180.79	523.73	−342.94
0.40	190.57	538.59	−348.02
0.50	140.58	435.05	−294.46
0.60	126.15	400.86	−274.71
0.70	79.05	298.71	−219.65
Average	141.79	441.62	−299.83

Overall, the findings demonstrate that the pyrolysis of OPEFB pellets is a potentially practical route for potential energy recovery. It is envisaged that the efficient pre-treatment, pelletisation, and valorisation of OPEFB will address the current challenges of disposal and management encountered by the palm oil industry in Malaysia. Therefore, the valorisation of OPEFB pellets into clean biofuels and bioenergy could well be a future indicator to the success of the National Biomass Strategy (NBS-2020) and the Fifth Fuel Policy (5FP) of Malaysia.

4 Conclusions

The paper examined the physicochemical, thermal, kinetic, and thermodynamic fuel properties of oil palm empty fruit bunch (OPEFB) pellets. The fuel characteristics revealed the OPEFB pellets: carbon (C), hydrogen (H), oxygen (O), volatile matter (VM), and fixed carbon (FC) are contained in high proportions compared to moisture (M) and ash (A) content along with the pollutant precursor elements nitrogen (N) and sulphur (S). The low proportions of N and S indicate OPEFB pellets are environmentally friendly solid biofuels for conversion and energy recovery, whereas the high C, H, VM, and FC contribute to the heating value of the OPEFB pellets. The morphological analysis revealed the OPEFB pellets are a porous material containing a dense network of various polymeric fibres, whereas the ash contains regularly shaped agglomerates with fine-textured and smooth surfaces. The mineralogical analysis revealed the OPEFB pellets and ash contain high metal and metal oxides detected in various concentrations. However, the functional group analysis revealed the chemical structure of OPEFB pellets consists of alcohols, aldehydes, aliphatic, aromatics, esters, and ketone compounds. The thermal properties revealed the OPEFB pellets are highly reactive, resulting in high loss of mass and low mass residuals during TGA. The thermal decomposition occurred in three (3) stages, namely drying, devolatilization, and char degradation. The findings confirmed that high heating rates significantly influenced thermal degradation behaviour and TPCs. Kinetic analysis indicated that activation energy (E_a) and frequency factor (A) fluctuated significantly showing for both FWO and KAS models. The multicomponent analysis revealed holocellulose, lignin, and other lignocellulosic components. Thermodynamic analysis indicated that thermal decomposition occurred through an intermediate step (activated complex) and characterised by highly complex, random, and multiphase first-order reactions. Lastly, the study demonstrated the valorisation of OPEFB pellets through pyrolysis is a potentially

practical route for sustainable biofuels, biomaterials, and bioenergy as envisioned by the NBS-2020 national policy of Malaysia.

References

1. Kushairi A, Ong-Abdullah M, Nambiappan B, Hishamuddin E, Bidin MNIZ, Ghazali R, Subramaniam V, Sundram S, Parveez GKA (2019) Oil palm economic performance in Malaysia and R&D Progress in 2018. J Oil Palm Res 31(2):165–194

2. Nambiappan B, Ismail A, Hashim N, Ismail N, Nazrima S, Idris NAN, Omar N, Saleh K, Hassan NAM, Kushairi A (2018) Malaysia: 100 years of resilient palm oil economic performance. J Oil Palm Res 30(1):13–25

3. AIM (2013) National Biomass Strategy 2020. New wealth creation for Malaysia's palm oil industry, vol 2.0, 2nd edn. Agensi Inovasi Malaysia (AIM), Kuala Lumpur

4. Chew JJ, Soh M, Sunarso J, Yong S-T, Doshi V, Bhattacharya S (2019) Gasification of torrefied oil palm biomass in a fixed-bed reactor: effects of gasifying agents on product characteristics. J Energy Inst. https://doi.org/10.1016/j.joei.2019.05.010

5. Sukiran MA, Abnisa F, Daud WMAW, Bakar NA, Loh SK (2017) A review of torrefaction of oil palm solid wastes for biofuel production. Energy Convers Manag 149:101–120

6. Ruksathamcharoen S, Chuenyam T, Stratong-on P, Hosoda H, Ding L, Yoshikawa K (2019) Effects of hydrothermal treatment and pelletizing temperature on the mechanical properties of empty fruit bunch pellets. Appl Energy 251:113385

7. Nasrin A, Ma A, Mohamad S, Choo Y, Rohaya M, Azali A (2006) Production of palm-based biomass briquettes. Malaysian Palm Oil Board Information Series. http://palmoilis.mpob.gov.my/publications/TOT/TT-330.pdf

8. Hamzah N, Tokimatsu K, Yoshikawa K (2019) Solid fuel from oil palm biomass residues and municipal solid waste by hydrothermal treatment for electrical power generation in Malaysia: a review. Sustainability 11(4):1060

9. Johari A, Nyakuma BB, Nor SHM, Mat R, Hashim H, Ahmad A, Zakaria ZY, Abdullah TAT (2015) The challenges and prospects of palm oil based biodiesel in Malaysia. Energy 81:255–261

10. Lai O-M, Tan C-P, Akoh CC (2016) Palm oil: production, processing, characterization, and uses. Technology & Engineering AOCS Press, USA

11. Chiew YL, Shimada S (2013) Current state and environmental impact assessment for utilizing oil palm empty fruit bunches for fuel, fiber and fertilizer–a case study of Malaysia. Biomass Bioenergy 51:109–124

12. Krishnan Y, Bong CPC, Azman NF, Zakaria Z, Abdullah N, Ho CS, Lee CT, Hansen SB, Hara H (2017) Co-composting of palm empty fruit bunch and palm oil mill effluent: microbial diversity and potential mitigation of greenhouse gas emission. J Clean Prod 146:94–100

13. Nasution MA, Wibawa DS, Ahamed T, Noguchi R (2018) Selection of palm oil mill effluent treatment for biogas generation or compost production using an analytic hierarchy process. J Mater Cycles Waste Manag 20(2):787–799

14. Ashikin NSSN, Djalaluddin A, Yusuff S, Khalil HA, Syakir MI (2019) Empty fruit bunch-seaweed biocomposite as potential soil

15. erosion mitigation material for oil palm plantation. BioResources 14(3):5438–5450

16. Abdullah M, Nazir M, Raza M, Wahjoedi B, Yussof A (2016) Autoclave and ultra-sonication treatments of oil palm empty fruit bunch fibers for cellulose extraction and its polypropylene composite properties. J Clean Prod 126:686–697

17. Lee SW, Oh C, Zain M, Yahya N The use of oil palm fiber as additive material in concrete. In: IOP Conference Series: Materials Science and Engineering, 2018. vol 4. IOP Publishing, p 042012

18. Harmaen AS, Khalina A, Azowa I, Hassan MA, Tarmian A, Jawaid M (2015) Thermal and biodegradation properties of poly (lactic acid)/fertilizer/oil palm fibers blends biocomposites. Polym Compos 36(3):576–583

19. Idris SS, Rahman NA, Ismail K (2012) Combustion characteristics of Malaysian oil palm biomass, sub-bituminous coal and their respective blends via thermogravimetric analysis (TGA). Bioresour Technol 123:581–591. https://doi.org/10.1016/j.biortech.2012.07.065

20. Chin K, H'ng P, Maminski M, Go W, Lee C, Raja-Nazrin R, Khoo P, Ashikin S, Halimatun I (2018) Additional additives to reduce ash related operation problems of solid biofuel from oil palm biomass upon combustion. Ind Crop Prod 123:285–295

21. Ruksathamcharoen S, Chuenyam T, Ajiwibowo MW, Yoshikawa K (2019) Thermogravimetric analysis of combustion characteristics and kinetics of hydrothermally treated and washed empty fruit bunch. Biofuels:1–10. https://doi.org/10.1080/17597269.2018.1564482

22. Lahijani P, Zainal ZA (2011) Gasification of palm empty fruit bunch in a bubbling fluidized bed: a performance and agglomeration study. Bioresour Technol 102(2):2068–2076. https://doi.org/10.1016/j.biortech.2010.09.101

23. Mastuli MS, Kamarulzaman N, Kasim MF, Sivasangar S, Saiman MI, Taufiq-Yap YH (2017) Catalytic gasification of oil palm frond biomass in supercritical water using MgO supported Ni, Cu and Zn oxides as catalysts for hydrogen production. Int J Hydrog Energy 42(16):11215–11228. https://doi.org/10.1016/j.ijhydene.2017.02.174

24. Talero G, Rincón S, Gómez A (2019) Biomass torrefaction in a standard retort: a study on oil palm solid residues. Fuel 244:366–378

25. Fuad MAHM, Ismail AR, Nyakuma BB, Khalis M, Faizal HM (2018) Torrefaction of hydrotreated palm kernel shell and Mesocarp fiber mixture. J Mekanikal 41(1):69–77. https://jurnalmekanikal.utm.my/index.php/jurnalmekanikal/article/view/325/322

26. Nasrin A, Vijaya S, Loh S, Astimar A, Lim W (2017) Quality compliance and environmental impact assessment of commercial empty fruit bunch (EFB) pellet fuel in Malaysia. J Oil Palm Res 29(4):570–578

27. Nyakuma BB, Ahmad A, Johari A, Abdullah TA, Oladokun O, Alkali H (2017) Fluidised bed gasification and chemical exergy analysis of pelletised oil palm empty fruit bunches. Chem Eng Trans 56(1):1159–1164

28. Basu P (2018) Biomass gasification, pyrolysis and torrefaction: practical design and theory. Academic Press, Canada. https://doi.org/10.1016/C2011-0-07564-6

29. Cancela A, Pérez L, Febrero A, Sánchez A, Salgueiro J, Ortiz L (2019) Exploitation of Nannochloropsis gaditana biomass for biodiesel and pellet production. Renew Energy 133:725–730

30. Olugbade T, Ojo O, Mohammed T (2019) Influence of binders on combustion properties of biomass briquettes: a recent review. BioEnergy Res 12(2):241–259

31. Mostafa ME, Hu S, Wang Y, Su S, Hu X, Elsayed SA, Xiang J (2019) The significance of pelletization operating conditions: an

analysis of physical and mechanical characteristics as well as energy consumption of biomass pellets. Renew Sust Energ Rev 105: 332–348

31. Kumar Singh R, Sarkar A, Chakraborty JP (2019) Effect of torrefaction on the physicochemical properties of pigeon pea stalk (Cajanus cajan) and estimation of kinetic parameters. Renew Energy 138:805–819

32. Szwaja S, Magdziarz A, Zajemska M, Poskart A (2019) A torrefaction of Sida hermaphrodita to improve fuel properties. Advanced analysis of torrefied products. Renew Energy 141:894–902

33. Shimadzu Corporation (2013) Energy dispersive X-ray fluorescence spectrometer EDX-7000/8000. Shimadzu Corporation, Japan. http://bit.ly/2B3qtDI. Accessed 23rd November 2017

34. Slopiecka K, Bartocci P, Fantozzi F (2012) Thermogravimetric analysis and kinetic study of poplar wood pyrolysis. Appl Energy 97:491–497. https://doi.org/10.1016/j.apenergy.2011.12.056

35. Açıkalın K (2011) Thermogravimetric analysis of walnut shell as pyrolysis feedstock. J Therm Anal Calorim 105(1):145–150. https://doi.org/10.1007/s10973-010-1267-x

36. Hattingh BB, Everson RC, Neomagus HW, Bunt JR, Van Niekerk D, Ashton BP (2014) Modeling the nonisothermal devolatilization kinetics of typical south African coals. Energy Fuel 28(2):920–933

37. Oladokun O, Ahmad A, Abdullah T, Nyakuma B, Bello A-H, Al-Shatri A (2016) Multicomponent devolatilization kinetics and thermal conversion of Imperata cylindrica. Appl Therm Eng 105:931–940

38. Maia AAD, de Morais LC (2016) Kinetic parameters of red pepper waste as biomass to solid biofuel. Bioresour Technol 204:157–163

39. Yoo H-M, Park S-W, Seo Y-C, Kim K-H (2019) Applicability assessment of empty fruit bunches from palm oil mills for use as biosolid refuse fuels. J Environ Manag 234:1–7. https://doi.org/10.1016/j.jenvman.2018.11.035

40. Yoo H-M, Seo Y-C, Park S-W, Kang J-J, Choi HS, Oh C-H (2018) Removal effect of ash and metallic species by washing from empty fruit bunch byproducts in palm mills on pyrolytic characteristics to produce bio-crude oil. Waste Biomass Valoriz 9(3):491–502. https://doi.org/10.1007/s12649-016-9807-7

41. Basu P (2010) Biomass gasification and pyrolysis: practical design and theory. Academic Press (Elsevier), Burlington

42. Vassilev SV, Baxter D, Andersen LK, Vassileva CG (2010) An overview of the chemical composition of biomass. Fuel 89(5): 913–933. https://doi.org/10.1016/j.fuel.2009.10.022

43. Romero E, Quirantes M, Nogales R (2017) Characterization of biomass ashes produced at different temperatures from olive-oil-industry and greenhouse vegetable wastes. Fuel 208(supplement C):1–9. https://doi.org/10.1016/j.fuel.2017.06.133

44. Basu P (2006) Combustion and gasification in fluidized beds. CRC press, Burlington

45. Vassilev SV, Vassileva CG, Vassilev VS (2015) Advantages and disadvantages of composition and properties of biomass in comparison with coal: an overview. Fuel 158:330–350

46. Awosusi AA, Ayeni AO, Adeleke R, Daramola MO (2017) Biocompositional and thermodecompositional analysis of South African agro-waste corncob and husk towards production of biocommodities. Asia-Pacific J Chem Eng. https://doi.org/10.1002/apj.2138

47. Mettanant V, Basu P, Butler J (2009) Agglomeration of biomass fired fluidized bed gasifier and combustor. Can J Chem Eng 87(5):656–684

48. Mohammed MAA, Salmiaton A, Wan Azlina WAKG, Mohamad Amran MS (2012) Gasification of oil palm empty fruit bunches: a characterization and kinetic study. Bioresour Technol 110:628–636. https://doi.org/10.1016/j.biortech.2012.01.056

49. Razmi FA, Ngadi N, Wong S, Inuwa IM, Opotu LA (2019) Kinetics, thermodynamics, isotherm and regeneration analysis of chitosan modified pandan adsorbent. J Clean Prod 231:98–109. https://doi.org/10.1016/j.jclepro.2019.05.228

50. Periyasamy S, Manivasakan P, Jeyaprabha C, Meenakshi S, Viswanathan N (2019) Fabrication of nano-graphene oxide assisted hydrotalcite/chitosan biocomposite: an efficient adsorbent for chromium removal from water. Int J Biol Macromol 132:1068–1078. https://doi.org/10.1016/j.ijbiomac.2019.03.232

51. Babiker E, Al-Ghouti MA, Zouari N, McKay G (2019) Removal of boron from water using adsorbents derived from waste tire rubber. J Environ Chem Eng 7(2):102948. https://doi.org/10.1016/j.jece.2019.102948

52. Wong S, Lee Y, Ngadi N, Inuwa IM, Mohamed NB (2018) Synthesis of activated carbon from spent tea leaves for aspirin removal. Chin J Chem Eng 26(5):1003–1011. https://doi.org/10.1016/j.cjche.2017.11.004

53. Laksmono JA, Sudibandriyo M, Saputra AH, Haryono A (2019) Structured polyvinyl alcohol/zeolite/carbon composites prepared using supercritical fluid extraction techniques as adsorbent for bioethanol dehydration. Int J Chem Eng 2019:11. https://doi.org/10.1155/2019/6036479

54. Zzeyani S, Mikou M, Naja J, Bouyazza L, Fekkar G, Aiboudi M (2019) Assessment of the waste lubricating oils management with antioxidants vegetables extracts based resources using EPR and FTIR spectroscopy techniques. Energy 180:206–215. https://doi.org/10.1016/j.energy.2019.05.007

55. Chong CT, Mong GR, Ng J-H, Chong WWF, Ani FN, Lam SS, Ong HC (2019) Pyrolysis characteristics and kinetic studies of horse manure using thermogravimetric analysis. Energy Convers Manag 180:1260–1267. https://doi.org/10.1016/j.enconman.2018.11.071

56. Yiin CL, Yusup S, Quitain AT, Uemura Y, Sasaki M, Kida T (2018) Thermogravimetric analysis and kinetic modeling of low-transition-temperature mixtures pretreated oil palm empty fruit bunch for possible maximum yield of pyrolysis oil. Bioresour Technol 255:189–197

57. El-Shafei AM, Adel AM, Ibrahim AA, Al-Shemy MT (2019) Dual functional jute fabric biocomposite with chitosan and phosphorylated nano-cellulose (antimicrobial and thermal stability). Int J Biol Macromol 124:733–741. https://doi.org/10.1016/j.ijbiomac.2018.11.137

58. Abrishami F, Chizari M, Zohari N, Pourmosavi SA (2019) Study on thermal stability and decomposition kinetics of Bis (2, 2-dinitropropyl) Fumarate (BDNPF) as a melt cast explosive by model-free methods. Propellants, Explosives, Pyrotechnics

59. Nyakuma BB, Ahmad A, Johari A, Tuan TA, Oladokun O, Aminu DY (2015) Non-isothermal kinetic analysis of oil palm empty fruit bunch pellets by thermogravimetric analysis. Chem Eng Trans 45: 1327–1332

60. Sun WG, Zhao H, Yan HX, Sun BB, Dong SS, Zhang CW, Qin S (2012) Pyrolysis characteristics and kinetics of Jerusalem artichoke stalk using thermogravimetric analysis. Energy Sourc A 34(7):626–635. https://doi.org/10.1080/15567036.2011.615006

61. Tian M, He H, Wang B-B, Wang X, Liu Y, Jiang F-L (2019) A reaction-based turn-on fluorescent sensor for the detection of Cu (II) with excellent sensitivity and selectivity: synthesis, DFT calculations, kinetics and application in real water samples. Dyes Pigments 165:383–390. https://doi.org/10.1016/j.dyepig.2019.02.043

62. Zsako J (1976) The kinetic compensation effect. J Therm Anal Calorim 9(1):101–108

63. Koppejan J, Van Loo S (2012) The handbook of biomass combustion and co-firing. Biomass Conversion, Routledge

64. Nyakuma BB, Ahmad A, Johari A, Tuan Abdullah TA, Oladokun O, Uthman H, Halim M (2016) Thermal decomposition kinetics of torrefied oil palm empty fruit bunch briquettes. Chem Chem Technol 10(3):325–328

65. Miura K, Maki T (1998) A simple method for estimating f(E) and k0(E) in the distributed activation energy model. Energy Fuel 12(5): 864–869. https://doi.org/10.1021/ef970212q

66. Rahman MA, Hopke PK (2016) Mechanistic pathway of carbon monoxide off-gassing from wood pellets. Energy Fuel 30(7):5809–5815

67. Mitchual SJ, Katamani P, Afrifa KA (2019) Fuel characteristics of binder free briquettes made at room temperature from blends of oil palm mesocarp fibre and Ceiba pentandra. Biomass Convers Biorefin: 9: 541. https://doi.org/10.1007/s13399-019-00410-8

68. Christoforou E, Fokaides PA (2019) Solid biofuels in trading form in global markets. In: Advances in Solid Biofuels. Springer, pp 57–68. Green Energy and Technology. Springer, Cham, Switzerland. https://doi.org/10.1007/978-3-030-00862-8_4